Improving operational ocean color coverage using a merged atmospheric correction approach

Dimitry Van der Zande*[a], Quinten Vanhellemont[a], Kerstin Stelzer[b], Carole Lebreton[b], Antoine Dille[a], João Cardoso dos Santos[c], Martin Böttcher[b], Dieter Vansteenwegen[d], Carsten Brockmann[b]

[a]Royal Belgian Institute of Natural Sciences, Vautierstraat 29, Brussels, Belgium
[b]Brockmann Consult, Chrysanderstraße 1, Hambrug, Germany
[c]Instituto Nacional de Pesquisas Espaciais, Av. dos Astronautas 1.758, São José dos Campos, Brazil
[d]Flanders Marine Institute, Wandelaarkaai 7, Ostend, Belgium

ABSTRACT

High-quality satellite-based ocean color products derived from Sentinel-2/MSI and Sentinel-3/OLCI provide valuable support and insights in the management and monitoring of coastal ecosystems. The primary ocean color variable is the spectral Remote Sensing Reflectance (RRS), obtained after applying atmospheric correction (AC) on satellite products. AC algorithms, such as C2RCC and ACOLITE/DSF are all well capable of generating RRS products over coastal waters. The question of which approach to choose is important and not obvious, especially considering different water (e.g. turbid, clear or CDOM rich waters) and atmospheric conditions (e.g. sun glint, low sun angles) which can occur in coastal waters. To improve the operational ability to achieve high quality RRS spectra for a maximum number of pixels and yet retain the ability to deal with both unusual water conditions and challenging atmospheric conditions, we present the merged use of two algorithms: C2RCC and ACOLITE/DSF. Combining the two approaches yet required a comprehensive, region independent and pixel-based automatic switching scheme, along with a technique for achieving a seamless transition between the two algorithms. We here used the green-NIR ratio, which offers a clear indication of the saturation of the C2RCC outputs for the most reflective band (i.e., the RRS560), at a level where ACOLITE/DSF typically performs accurately, combined with a weighted transition between the two methods. The approach was applied to both Sentinel-2/MSI and Sentinel-3/OLCI products and validated using autonomous WATERHYPERNET stations located in Oostende (RT1, Belgium) and Venice (AAOT, Italy), showing an improved quality of the RRS products compared to using the ACs independently. The best results are obtained for the merged approach in the bands 443nm to 709nm for both Sentinel-2/MSI (<21% MAPE with a 0.004 RMSD and slopes between 0.93 and 0.98) and Sentinel-3/OLCI (<23% MAPE with a 0.003 RMSD and slopes between 0.91 and 0.98) which have generally the highest reflectance range, and which are generally of interest to retrieve turbidity in low to moderately turbid waters.

Keywords: Coastal waters, Atmospheric correction, Validation, Sentinel-2/MSI, Sentinel-3/OLCI, PANTHYR, ACOLITE-DSF, C2RCC

1. INTRODUCTION

Ocean color remote sensing has become a mature science, with operational products based on Sentinel-2/MSI and Sentinel-3/OLCI data providing day-to-day, global-scale information at spatial resolutions of tens to a few hundred meters. Many of these products are available as open access data through Copernicus Data Space Ecosystem and the Copernicus Marine service, providing valuable support and insights for the management and monitoring of coastal marine ecosystems [1]. One of the major challenges in ocean-color remote sensing is correct atmospheric correction (AC) to obtain accurate estimates of the Remote Sensing Reflectance (RRS) at every pixel [2]. [2]From the RRS it is possible to derive biogeophysical (e.g. chlorophyll-a concentrations [3]) and transparency (e.g. suspended particulate matter concentration [4][5]) variables that are at the core of ocean and coastal environment management and monitoring. The AC procedure is succession of processing steps including:

- Correction for absorbing atmospheric gases;
- Correction for molecular ("Rayleigh") scattering in the atmosphere;

*dvanderzande@naturalsciences.be; https://odnature.naturalsciences.be/remsem/

- Correction for aerosol (and multiple aerosol-Rayleigh) scattering in the atmosphere, including potentially absorbing aerosols and taking account of the fact that water reflectance in the near infrared is not negligible ("turbid water effects");
- Correction for reflectance of skyglint (Rayleigh and aerosol) at the air-water interface, often included in the "aerosol" and "Rayleigh" scattering corrections;
- Correction for reflectance of direct sunglint at the air-water interface (still topic of evolution);

AC algorithms, including C2RCC [6][7], ACOLITE-DSF [2], iCOR [8] and POLYMER [9][10] were initially developed for specific water conditions, such as turbid and inland waters, Case 2 waters, land surfaces, and sun-glinted Case 1 waters, but the range of water types covered by these algorithms have since been generally expanded to cover more water types. Yet, a very large diversity in water types are typical in coastal areas (e.g., in the vicinity of river estuaries), while the recent ACIX-2 algorithm intercomparison [11] for water ACs showed that there is no clear optimal approach for all the tested water types. Choosing an appropriate approach is therefore both critical but not straightforward and given that all atmospheric correction methods are constantly being improved and refined, the optimal option may change over time.

[11]Based on their approach, the ACs reviewed can be divided into two groups. AC algorithms such as ACOLITE-DSF make no assumption about the water reflectance, allowing the estimate of atypical water reflectance spectra that correspond to optical properties not present in a typical water reflectance model or might lead to an ill-defined mathematical problem with multiple solutions for the more usual water conditions. However, the disadvantage of this approach is that some atmospheric conditions (e.g. severely sun glinted pixels) may be just too challenging. On the other hand, AC algorithms such as C2RCC have an underlying water reflectance model that assumes that water reflectance will fit some known form (albeit with a certain number of degrees of freedom). The main advantage of the latter approach is that the additional information provided by the constraint on the water reflectance spectra enables a solution to be obtained even in very challenging situations such as high sun glint - i.e. these approaches (unless they fail completely) will always produce an RRS spectrum that looks like water. Further, they can even be relatively insensitive to sensor calibration errors and produce a water spectrum even in case of very low reflectance level.

Using a single AC for a domain is the most straightforward (and common) approach, as there are certain characteristics that occur more frequently in certain domains: e.g. the Southern North Sea is characterized by turbid coastal waters (case 2 waters) while the Mediterranean Sea is mostly characterized by clear waters (case 1 waters) and is more exposed to sun glint because of the lower sun zenith angle. However, there are also many exceptions, e.g. high sun zenith angle conditions occur everywhere in winter, sun glint contaminates also much of the more Northern regions in summer, etc. Nor is there a clear spatial demarcation of water types even within a domain: turbid waters from river plumes vary in spatial extent, high biomass algae blooms vary strongly both in time and space, sun glint depends also on local wind speed. To maximize the ability to obtain high quality RRS spectra for a maximum number of pixels and yet retain the ability to deal with both exceptional water conditions and very challenging atmospheric conditions within a domain we suggest using two complementary ACs, C2RCC (version 1.0, normal NN) and ACOLITE/DSF (version November 2022), in combination with an automatic pixel-based switching/merging approach based on the optical characteristics of the water at the pixel level. The approach is demonstrated on both Sentinel-2/MSI and Sentinel-3/OLCI images and validated by exploiting RRS measured at autonomous WATERHYPERNET stations located in Oostende (RT1, Belgium) and Venice (AOOT, Italy) and directly compared to C2RCC and ACOLITE outputs.

2. DATA AND METHODS

2.1 Study areas

This study focuses on two coastal water sites: the Belgian Coastal Zone (BCZ) and the Gulf of Venice (Italy). The BCZ is a relatively shallow (<50 m) well-mixed shelf sea, connected to the North Sea in the north and to the English Channel in the west [12]. It is characterized by a relatively high suspended sediment concentration, with a gradient from several hundreds of g/m^3 nearshore to <1 g/m^3 in the offshore waters, inversely related to the bathymetry [4][5][13]. Strong tidal currents and the tidal resuspension of sediments is the main cause of the high turbidity in the nearshore area [14][15]. Annually recurring phytoplankton blooms are observed in spring and summer. These blooms are generally composed of

diatoms and *Phaeocystis globose* [16]. In recent years, blooms have been occurring earlier, likely in response to sea surface temperature increases and changes in nutrient outputs [17][18]. The water type is turbid coastal to turbid coastal with high organic content. The Gulf of Venice is located in the northern Adriatic Sea, where the ocean circulation is mainly influenced by the coastal southward flow of the North Adriatic current and a North Adriatic (cyclonic) gyre in autumn [19][20]. The site is also influenced by discharge from northern Adriatic rivers: Piave, Livenza and Tagliamento [21]. The water type can vary depending on wind and swell conditions from clear open sea to turbid coastal [22][23][24].

2.2 In situ data

Two autonomous PANTHYR systems [25] were deployed at the Acqua Alta Oceanographic Tower (AAOT, 45.3139°N, 12.5083°E) and at Research Tower 1 (RT1) near Oostende (RT1, 51.2464°N, 2.9193°E). Fig. 1 shows the location of RT1 in the turbid coastal waters around Oostende and the location of AAOT in coastal waters near Venice.

Figure 1. left: the location of the RT1 platform just in front of Oostende in the Belgian Coastal zone and right: the location of the AAOT platform just in front of Venice in the North Adriatic Sea. (Sentinel-2/MSI image taken on 2023-04-03)

The PANTHYR system has two TriOS RAMSES radiometers mounted on a pan-and-tilt head, one for up- and downwelling spectral radiances, and one with a cosine collector to measure spectral irradiance. The PANTHYR measures autonomously every 20 min at programmed relative azimuth angles to the sun. In the present study, measurements were made at a 270° azimuth angle. A measurement cycle consists of sequential scans of 3× spectral irradiance (Ed), 3× downwelling radiance (Ld), 11× upwelling radiance (Lu), 3×Ld and 3×Ed. Such a measurement cycle for a single azimuth angle takes about 1 min. Measurements are calibrated, dark current corrected, and resampled to a common wavelength grid, from 350 to 900 nm at 2.5 nm steps. Individual scans are subjected to a quality control as in [26] and then averaged to provide a single equivalent measurement, if at least 9/11 Ed and 5/6 of the Ld and Lu scans pass the quality control. RRS is then computed using:

$$RRS = \frac{L_w}{E_d} \qquad (1)$$

where *Lw* is the water-leaving radiance

$$L_w = L_u - \rho_f . L_d \qquad (2)$$

where ρ_f is the effective Fresnel coefficient linearly interpolated from [27] for the sun zenith angle at the time of measurement, and the wind speed retrieved from the National Centers for Environmental Prediction (NCEP) 1-degree global model [28]. Because of the hyperspectral measurements, one significant advantage of the PANTHYR datasets when compared to AERONET-OC [22] (which is typically used for validating ocean-colour satellites), is that the hyperspectral instrument permits the validation of all MSI and OLCI VNIR bands within the 400-900 nm range, including several near-infrared (NIR) bands not available with the AERONET-OC instrument. [22]RRS data were finally convolved to the relative spectral response functions of the MSI and OLCI instruments on Sentinel-3 A and B and Sentinel-2 A and B. Fig.

2 compares the rather turbid waters at RT1 (orange) with the clear waters to optically complex waters found at AOOT (Blue). At RT1 the 5–95 percentiles of RRS are 0.017–0.042 at 560nm, 0.007–0.030 at 665nm, and 0.006–0.029 at 709nm, with median values respectively 0.027, 0.017, and 0.015. At AAOT the 5–95 percentiles of RRS are 0.004–0.021 at 560nm, 0.001–0.005 at 665nm, and 0.0004–0.004 at 709nm, with median values respectively 0.008, 0.002, and 0.001. In the period from 2019-12-11 to 2023-08-01, 2660 and 3756 PANTHYR measurements made at 270∘ relative azimuth passing quality control were available for RT1 and AAOT respectively. Figs. 3 and 4 show the PANTHYR observations for both stations in 2020 for five spectral bands.
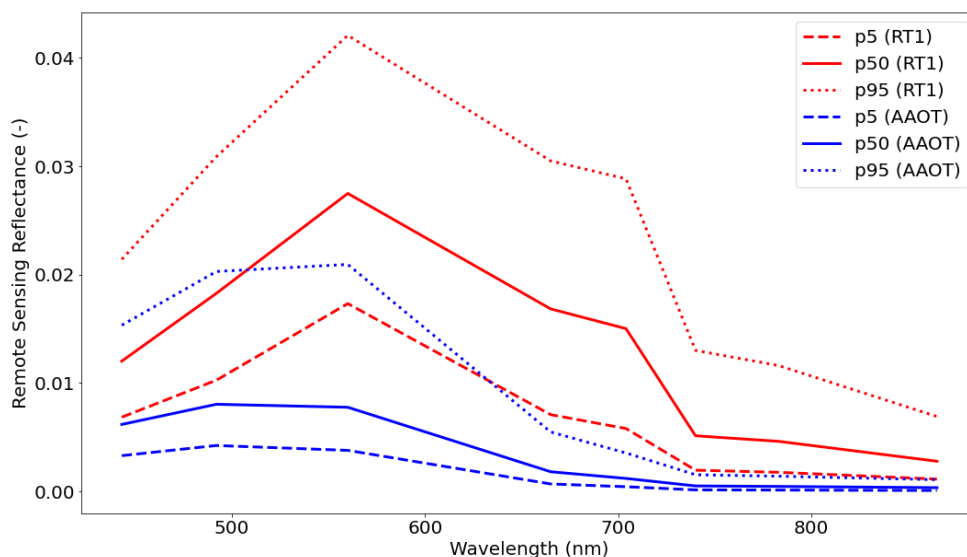

Figure 2. 5 (dashed), 50 (solid), and 95th (dotted) percentiles of the PANTHYR data convolved to the Sentinel-2/MSI relative spectral response functions, for the full archive of RT1 (red) and the AAOT (blue).
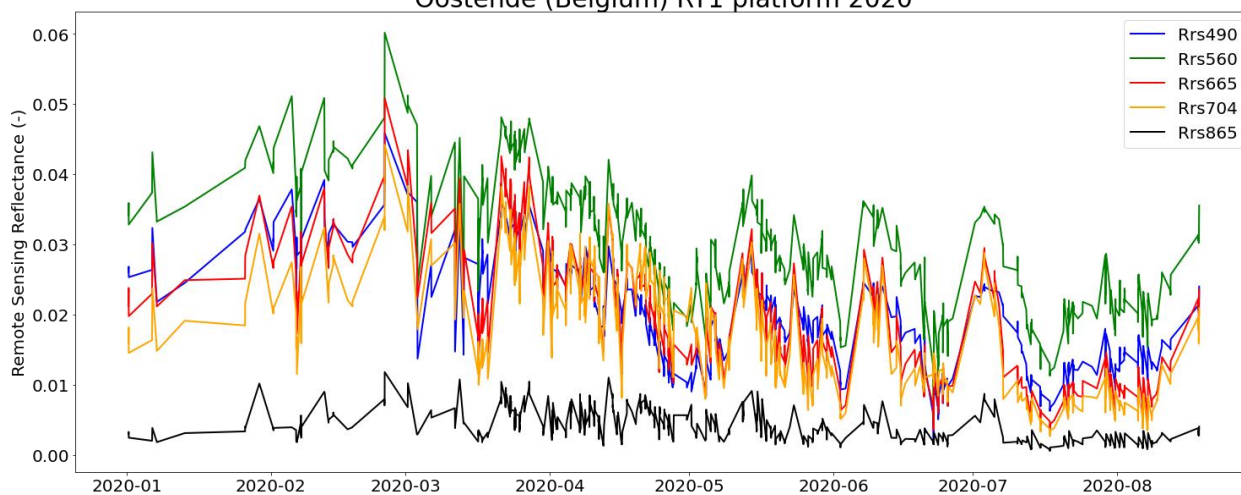

Figure 3. Timeseries of PANTHYR data convolved to the Sentinel-2/MSI RRS for five bands at the RT1 Site.
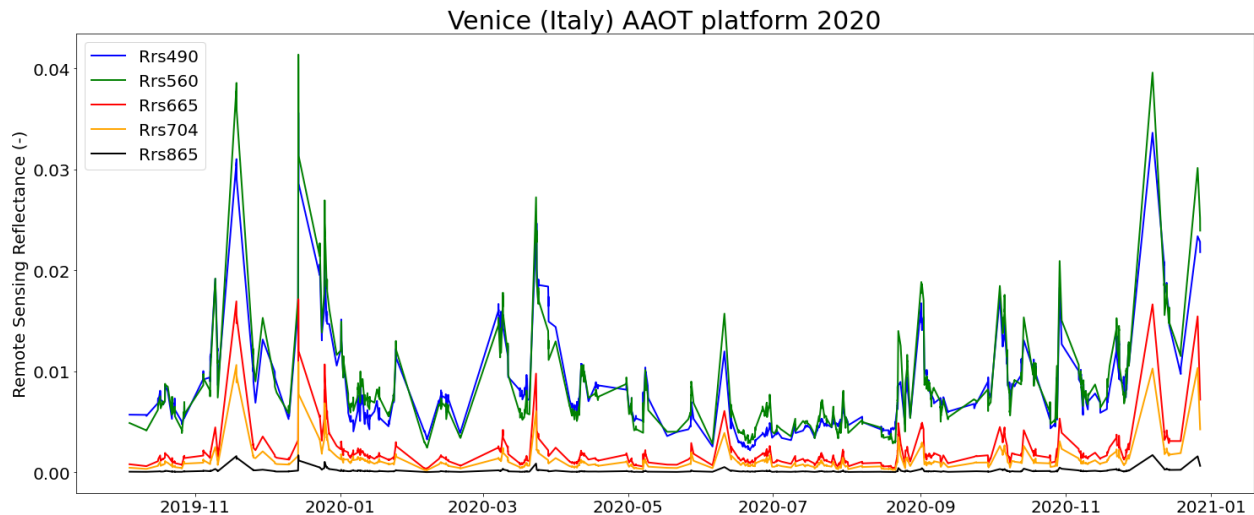
Figure 4. Timeseries of PANTHYR data convolved to the Sentinel-2/MSI RRS for five bands at the AAOT Site

The PANTHYR data is considered as pre-operational and is described in more detail in [25] and [29].

2.3 Satellite data

The Multi Spectral Instrument (MSI) is a multispectral radiometer carried on board Sentinel-2A (launched in 2015) and B (launched in 2017) with 13 bands in the 443–2200 nm spectral range with four bands at 10 m, six bands at 20 m and three bands at 60 m spatial resolution. In this study all bands were resampled to 60 m resolution. The two Sentinel-2 satellites in polar orbit can provide a 3-5 daily revisit time at the study sites. The Ocean and Land Colour Instrument (OLCI) is a multispectral radiometer carried on board Sentinel-3A (launched in 2016) and B (launched in 2018) with 21 bands in the 400–1020 nm spectral range at an approximately 300 m spatial resolution. The two satellites in polar orbit can provide a daily revisit time at the study sites.

The full processing chain was applied to both the Sentinel-2/MSI L1C and Sentinel-3/OLCI L1WFR products available on CREODIAS (https://creodias.eu/) and follows the general steps as applied in the Copernicus Marine Service, high-resolution coastal service (https://catalogue.marine.copernicus.eu/documents/QUID/CMEMS-HR-OC-QUID-009-201to212.pdf). In the first step of the processing chain the Pixel Identification is applied. This includes cloud masking and cloud shadow identification. However, there are other critical situations which are identified such floating vegetation, sub-pixel objects (ships, small islands and rocks), and the land-water distinction also needs to be performed taking temporary water bodies (e.g. intertidal areas, lagoons) into account. The IdePix software (v8.0.3 for Sentinel-2/MSI, v3.0.3 for Sentinel-3/OLCI), available as a SNAP (v8.0) processor, is used here, and is complemented by quality tests coming from the AC algorithms. IdePix uses several spectral tests of which the following flags were used to reject pixels: CLOUD, CLOUD_AMBIGUOUS, CLOUD_SURE, CLOUD_BUFFER, CLOUD_SHADOW, SNOW_ICE, CIRRUS_SURE, VEG_RISK, CLUSTERED_CLOUD_SHADOW, LAND.

In the next step two AC algorithms are applied:

- C2RCC: The C2RCC NN as provided in SNAP 8.0 with default settings (NN v.1.0). The c2rcc_flags dataset was used to reject pixels where flags Rtosa_OOR, Rhow_OOR were set.

- ACOLITE-DSF: The DSF version in ACOLITE was used to process L1 data from both sensors to RRS using a fixed aerosol optical thickness retrieved from the region of interest (ROI) centered on the measurement towers. The ACOLITE-DSF flags applied were SWIR_Water_clouds, Cirrus_clouds, TOA_treshold, and Rhow_neg.

2.4 Merging approach of Atmospheric Correction algorithms

C2RCC and ACOLITE-DSF are highly complementary because ACOLITE-DSF makes no assumption about the water reflectance and can therefore achieve good results even for atypical water types (e.g. turbid coastal waters, dredging plumes, unusual algae species, etc.) whereas C2RCC constrains the water reflectance to correspond to the training data,

always giving an RRS spectrum that looks like water. This extra information/constraint on water reflectance, embedded within the C2RCC approach, provides greater retrieval power in the most difficult circumstances (sun glint, highly absorbing waters) but at the expense of imposing a solution for RRS that may not correspond to reality. To improve the operational ability to obtain high quality RRS spectra for a maximum number of pixels and yet retain the ability to deal with both water conditions and challenging atmospheric conditions, we present the merged use of both AC algorithms.

The C2RCC to ACOLITE/DSF pixel-based switching is performed by means of band comparison of the RRS560 and RRS865 products (defined as $ratio_{green-nir}$) as provided by the C2RCC processor. The $ratio_{green-nir}$ can be modelled using a logarithmic regression curve which starts as linear for the smaller reflectance values, but bends at the point where the saturation of the most sensitive band (i.e. RRS560) occurs. C2RCC pixels which deviate from the logarithmic model are considered erroneous outputs. The ACOLITE/DSF processor has the ability to provide higher RRS ranges compared to C2RCC while being noisier for lower RRS values thus highlighting the complementary between the two approaches. The $ratio_{green-nir}$ value of 45 is selected as the transition point between C2RCC and ACOLITE/DSF products. To ensure a smooth transition between the different ACs, a weighted transition is applied between the $ratio_{green-nir}$ boundaries (Sb_{high} and Sb_{low}) of 50 and 40 based on the method described by [30]. The smooth transition between the ACs is triggered at the pixel level for waters where the RRS865 product from C2RCC is higher than 0.0005 sr^{-1} to avoid inclusion of noisy ACOLITE/DSF outputs in dark waters and uses these smoothing boundary values using the following weighting equation (Eq. 3):

$$if\ Rrs_{C2RCC\_865nm} > 0.0005\ then\ Rrs_{merged} = \alpha \times Rrs_{ACOLITE} + \beta \times Rrs_{C2RCC} \qquad (3)$$

With:

$$\alpha = \log\left(\frac{Sb_{high}}{ratio_{green-nir}}\right) \div \log\left(\frac{Sb_{high}}{Sb_{low}}\right) \qquad (4)$$

$$\beta = \log\left(\frac{ratio_{geen-nir}}{Sb_{low}}\right) \div \log\left(\frac{Sb_{high}}{Sb_{low}}\right) \qquad (5)$$

Note that the transition and smoothing interval are considered independent of the region as it is associated with the inherent limitations of C2RCC. Fig. 5 shows the resulting merged RRS560 product by combining the C2RCC and ACOLITE/DSF products with an indicator map (left) showing which AC algorithm was used for each pixel. The yellow zone highlights the region of the weighted transition between C2RCC and ACOLITE-DSF. Three locations are highlighted in the indicator map: 'x' in the ACOLITE-DSF zone (red) at the RT1 location; '2' in the transition zone (yellow); '3' in the C2RCC zone (blue). Fig. 6 shows for each of these locations the ACOLITE-DSF and merged spectra demonstrating the ability of the approach to retain the spectral shapes in the different situations.
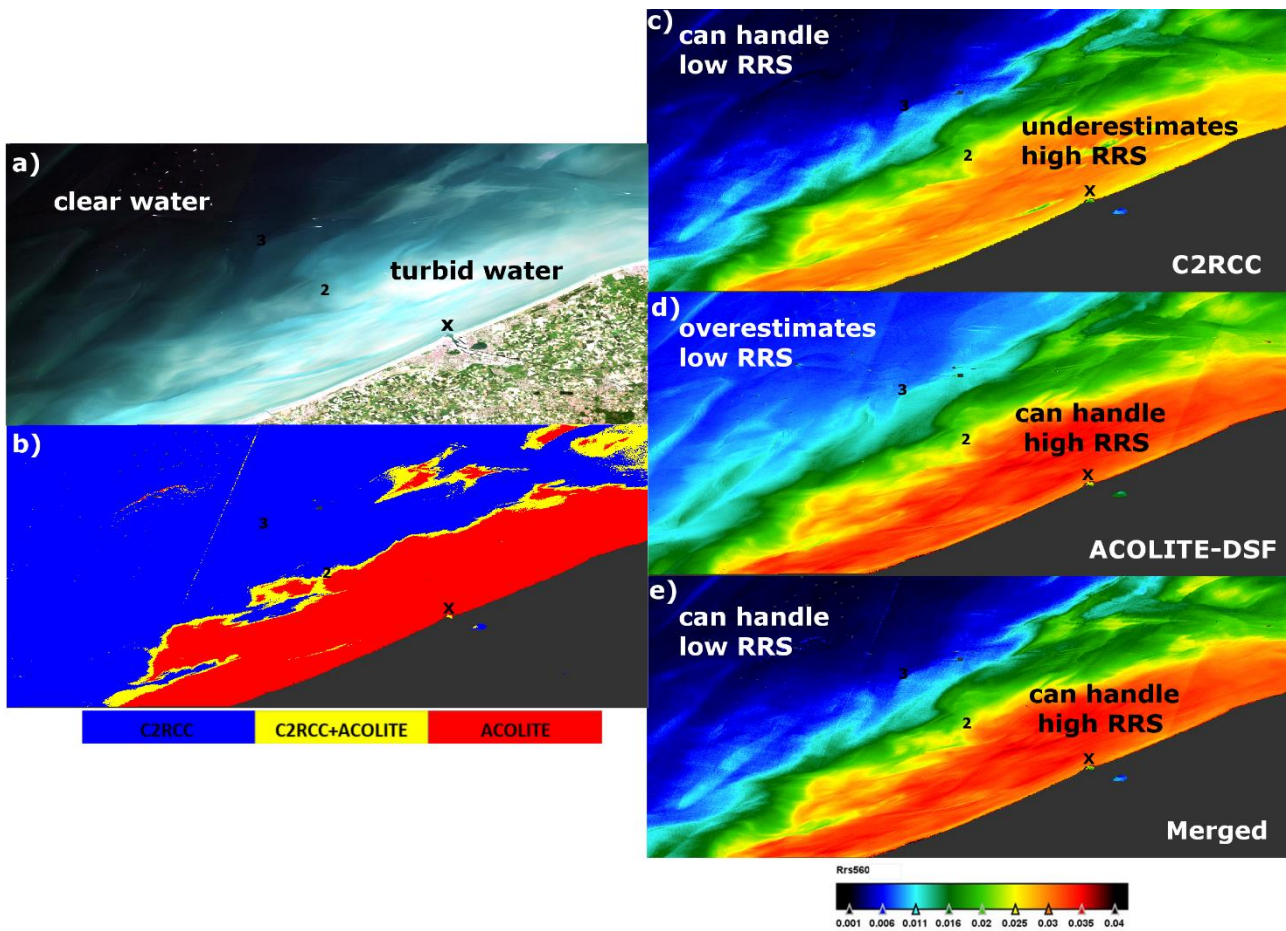
Figure 5. Sentinel-2B tile for Belgian Coastal Zone near the RT1 station (star) on 9/6/2023 represented by its RGB image (a) showing the transition from offshore clear waters into highly turbid waters near the coast. The RRS product for the 560nm band (RRS560) from C2RCC (c) shows realistic results in clear to moderately turbid waters but underestimates RRS in highly turbid waters. The RRS560 product from ACOLITE/DSF (d) shows better performance in the optically complex turbid waters but shows an overestimation of the RRS product at low RRS. (b) The indicator map for the Sentinel-2B tile shows which AC algorithm was used in the merged RRS560 product (e) which correctly estimates low and high RRS values. 'x' shows the RT1 location near Oostende and '2' and '3' highlight more locations for which spectra are plotted in figure 6.

2.5 Matchups

For the match-up extraction, a maximum time difference of 2 hours between in situ observation and satellite overpass was allowed. However, the high frequency measurement protocol from the in-situ measurement stations resulted in shorter time differences between in situ and satellite observations. The matchup validation protocol described by [31] was applied to remove erroneous matchups from the analysis. Macro-pixels of 3x3 60m pixels for MSI and 3x3 300m for OLCI were extracted from the L2 products. The RRS observations from the in-situ and satellite sensor were compared using the statistical parameters listed in table 1.
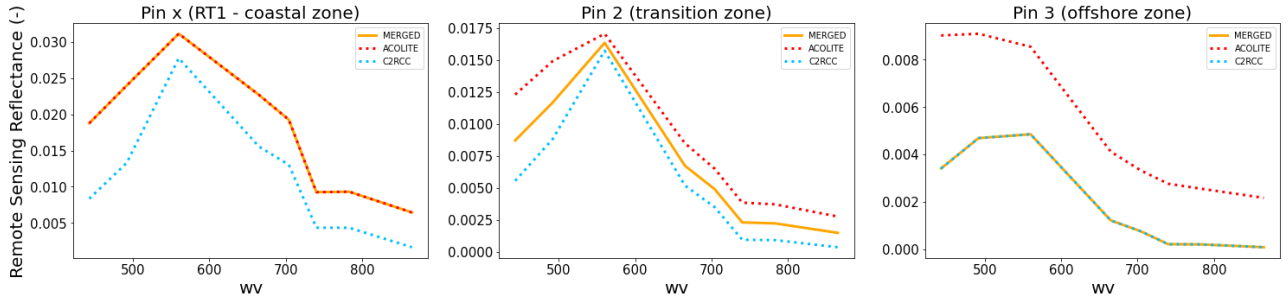
Figure 6. ACOLITE-DSF, C2RCC and merged spectra for three locations highlighted in Fig. 5: 'x' for RT1, '2' for the transition zone and '3' for the C2RCC zone.

Table 1. Metrics used to compare the estimated (satellite-based) $X_{i,j=1..N}^E$ dataset to a reference (in-situ) $X_{i,j=1..N}^M$ dataset.

Name	Definition
Estimated dataset mean ($\bar{X}^E$)	$$\bar{X}^E = \frac{1}{N} \sum_{i=1}^{N} X_i^E$$
Reference dataset mean ($\bar{X}^M$)	$$\bar{X}^M = \frac{1}{N} \sum_{i=1}^{N} X_i^M$$
Type-2 slope (S)	$$S = \frac{\sum_{i=1}^{N}(X_i^E - \bar{X}^E)^2 - \sum_{i=1}^{N}(X_i^M - \bar{X}^M)^2 + \left[\{\sum_{i=1}^{N}(X_i^E - \bar{X}^E)^2 - \sum_{i=1}^{N}(X_i^M - \bar{X}^M)^2\}^2 + 4\{\sum_{i=1}^{N}(X_i^E - \bar{X}^E)(X_i^M - \bar{X}^M)\}^2\right]^{\frac{1}{2}}}{2 \sum_{i=1}^{N}(X_i^E - \bar{X}^E)(X_i^M - \bar{X}^M)}$$
Type-2 intercept (i)	$$I = \bar{X}^E - S \cdot \bar{X}^M$$
Determination coefficient (r^2)	$$r^2 = \frac{[\sum_{i=1}^{N}(X_i^E - \bar{X}_i^E)(X_i^M - \bar{X}_i^M)]^2}{\sum_{i=1}^{N}(X_i^E - \bar{X}_i^E)^2 \sum_{i=1}^{N}(X_i^M - \bar{X}_i^M)^2}$$
Root Mean Square Difference (RMSD)	$$RMSD = \sqrt{\frac{\sum_{i=1}^{N}(X_i^E - X_i^M)^2}{N}}$$
Centre-pattern Root Mean Square Difference (cRMSD)	$$cRMSD = \sqrt{\frac{\sum_{i=1}^{N}\{[X_i^E - \bar{X}^E] - [X_i^M - \bar{X}^M]\}^2}{N}}$$
Bias	$$bias = \frac{1}{N} \sum_{i=1}^{N}(X_i^E - X_i^M)$$
Median Absolute Percentage Difference (MAPD)	$$MAPD = median\left(\left|\frac{X_i^E - X_i^M}{X_i^M}\right|\right)$$

3. RESULTS AND DISCUSSION

3.1 Sentinel-2 MSI RRS retrieval

Fig. 7 and 8 show the RRS matchups between Sentinel-2/MSI and the PANTHYR in situ instrument installed on RT1 and AAOT. In the deployment period between 2019-12-11 and 2023-08-01, 1080 MSI L1C images were available for processing, about equally distributed among the RT1 (528) and AAOT site (552), with 169 matchups (S2A: 78, S2B: 91) with the PANTHYR instrument which passed the quality flagging of the individual ACs (i.e. ACOLITE-DSF and C2RCC), IDEPIX quality flagging and the match-up quality flagging.

For C2RCC, the Mean Average Percentage Error (MAPE) is below 30% for all bands between 490 and 704 nm, with a MAPE of 15.72% for the 560nm band (i.e., the band with the largest observed reflectance range). The MAPE are the highest (>35%) for the shortest (443nm) and longest wavelengths (865nm), which can be attributed to the low data ranges. Additionally, the complexity of correcting the atmospheric path in the blue region contributes to the high MAPE at the 443nm wavelength. While plots for C2RCC show small scatter resulting in high regression coefficients (R^2) ranging from 0.76 to 0.98 for all bands between 490nm and 704nm. The slopes indicate a deviation from the 1:1 line with values from 0.56 to 0.86. The underestimation of the RRS products is especially noticeable for high RRS values (i.e., turbid waters).

For ACOLITE-DSF, the MAPE is below 43% for all bands between 490 and 704 nm, with a MAPE of 13.27% for the 560nm band. Here also, the MAPE are the highest (>45%) for the shortest (443nm) and longest wavelengths (865nm). The scatter plots of ACOLITE-DSF show slightly more spread compared to C2RCC resulting in regression coefficients (R^2) ranging from 0.82 to 0.95 for all bands between 490nm and 704nm. The matchups between satellite and in situ observations match the 1:1 line resulting in slopes between 0.85 to 0.92. Especially in the NIR bands (740nm to 865nm), the increased spread and bad matchups in the lower RRS values support the observation that ACOLITE-DSF struggles with RRS retrieval in clear waters while performing better in more reflective turbid waters.

Finally, when using the merged approach for atmospheric correction, the best performing bands are 492, 560, 665, and 704nm which are typically used for retrieval of turbidity and turbid water chlorophyll-a. For these bands the MAPE ranges between 12.68% and 21.60% with improvements compared to both ACOLITE-DSF and C2RCC ranging between 0.25% and 26.88%. Additionally, the merged approach shows an improvement as highlighted by regression coefficients (R^2) ranging from 0.87 to 0.95 and slopes between 0.92 to 0.98 for all bands between 490nm and 704nm improving the match with the 1:1 line for both the low and high RRS values.

Fig. 11 provides a graphical overview of band-specific statistical metrics (i.e. slope, MAPE, RMSE) for both the PANTHYR matchup analysis.

3.2 Sentinel-3 OLCI RRS retrieval

Fig. 9 and 10 show the RRS matchups between the Sentinel-3/OLCI and the PANTHYR instrument installed on RT1 and AAOT. In the deployment period between 2019-12-11 and 2023-08-01, 4300 OLCI L1FR images were available for processing, about equally distributed among the RT1 (2334) and AAOT site (1966), with 454 common matchups (S3A: 266, S3B: 188) with the PANTHYR instrument which passed the quality flagging of the individual ACs (i.e. ACOLITE-DSF and C2RCC), IDEPIX quality flagging and the match-up quality flagging.

For C2RCC, the MAPE is below 25% for all bands between 443 and 709nm, reaching 18.20% for the 560nm band (i.e. the band with the largest observed reflectance range). The MAPE are highest (>40%) for the longer wavelengths (779nm and 865nm). While the scatter plots for C2RCC show small scatter resulting in high regression coefficients (R^2) ranging from 0.65 to 0.95 for all bands between 443nm and 709nm, the slopes indicate a deviation from the 1:1 line with values from 0.71 to 0.94. The underestimation of the RRS products is especially noticeable in the higher RRS values (i.e., turbid waters). These findings are supported by [28] stating that C2RCC introduced artificial Red band chlorophyll-a absorption or reduced the presence of a real RedEdge feature which are both problematic for typical eutrophication monitoring applications in turbid waters.

For ACOLITE-DSF, the MAPE is below 33% for all bands between 443nm and 709 nm, reaching 12.92% for the 560nm. The MAPE are highest (>29%) for the longer wavelengths (779nm and 865nm), as a result of low data ranges. The scatter plots of ACOLITE-DSF show slightly more spread compared to C2RCC resulting in regression coefficients (R^2) ranging

from 0.47 to 0.89 for all bands between 490nm and 709nm. However, the matchups between satellite and in situ observations match the 1:1 line better compared to C2RCC resulting in slopes between 0.91 to 1.07. Especially in the NIR bands (740nm to 865nm), the increased spread and bad matchups in the lower RRS values support the observation that ACOLITE-DSF struggles with RRS retrieval in clear waters while performing better in more reflective turbid waters.

Finally, when using the merged approach for atmospheric correction, the best performing bands are 443, 492, 560, 665, and 709nm which are typically used for retrieval of turbidity and turbid water chlorophyll-a. For these bands the MAPE ranges between 12.68% and 21.60% with improvements compared to both ACOLITE-DSF and C2RCC ranging between 0.24% and 17.57%. Additionally, the merged approach shows an improvement as stated by the regression coefficients (R^2) ranging from 0.73 to 0.92 and slopes between 0.91 to 1.02 for all bands between 490nm and 709nm improving the match with the 1:1 line for both the low and high RRS values.

Fig. 12 provides a graphical overview of band-specific statistical metrics (i.e. slope, MAPE, RMSE) for the PANTHYR matchup analysis.
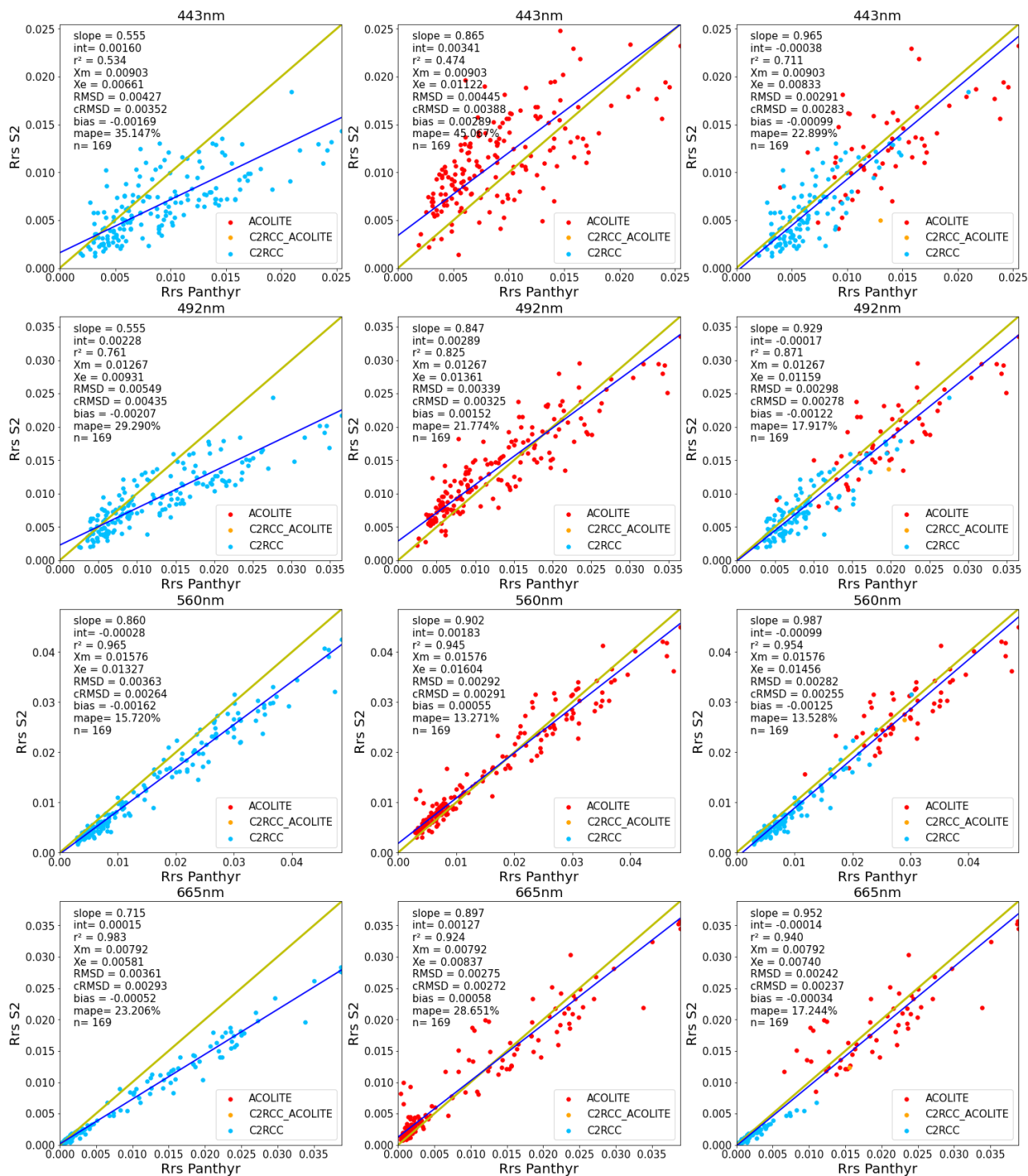
Figure 7. L3 daily MSI spectral RRS dataset in the visual bands against in situ observations obtained from the PANTHYR network for 2 stations: RT1 and AAOT as processed with C2RCC (left column), ACOLITE-DSF (middle column) and the merged approach (right column) with a color code showing which AC was used per matchup.
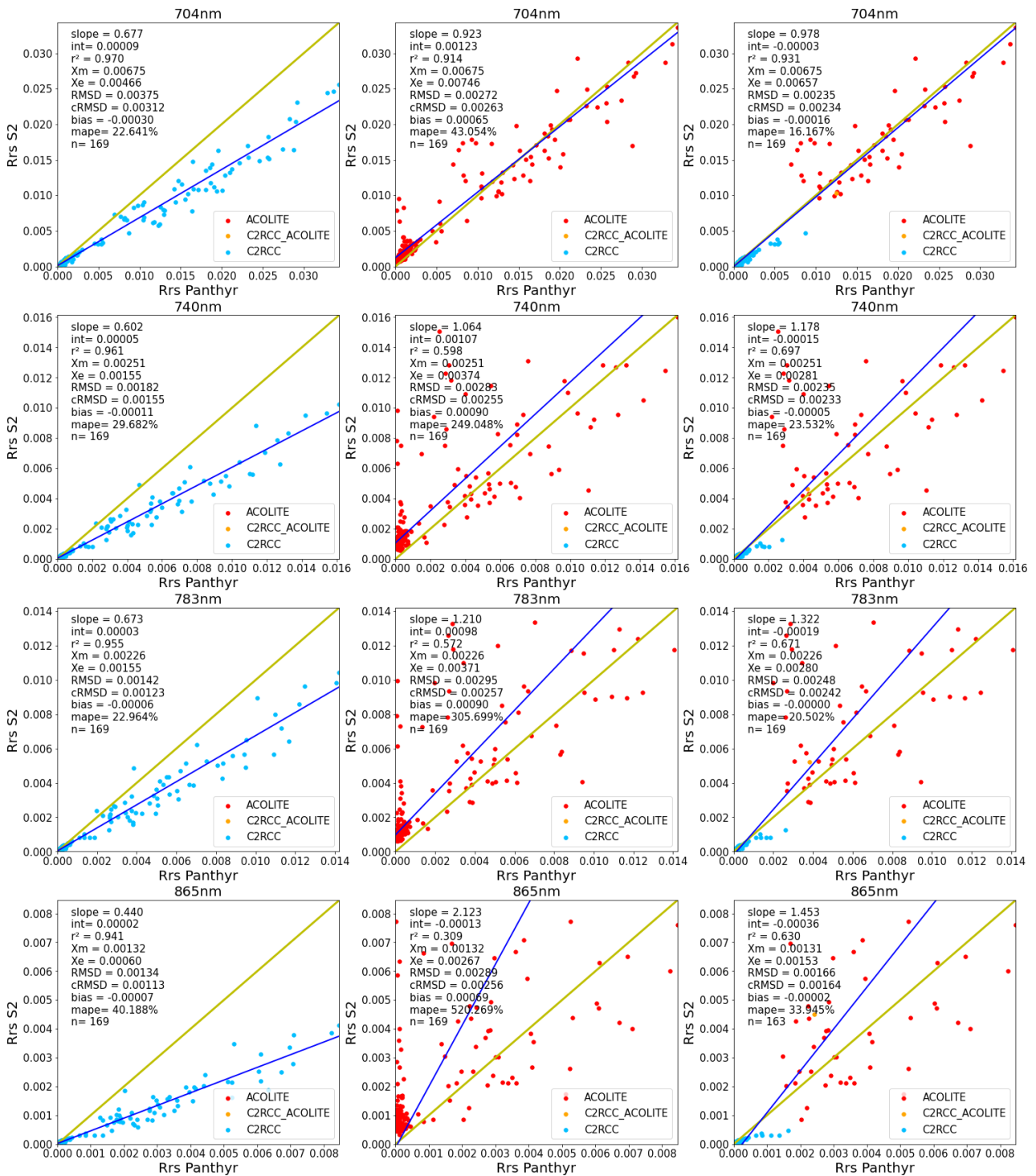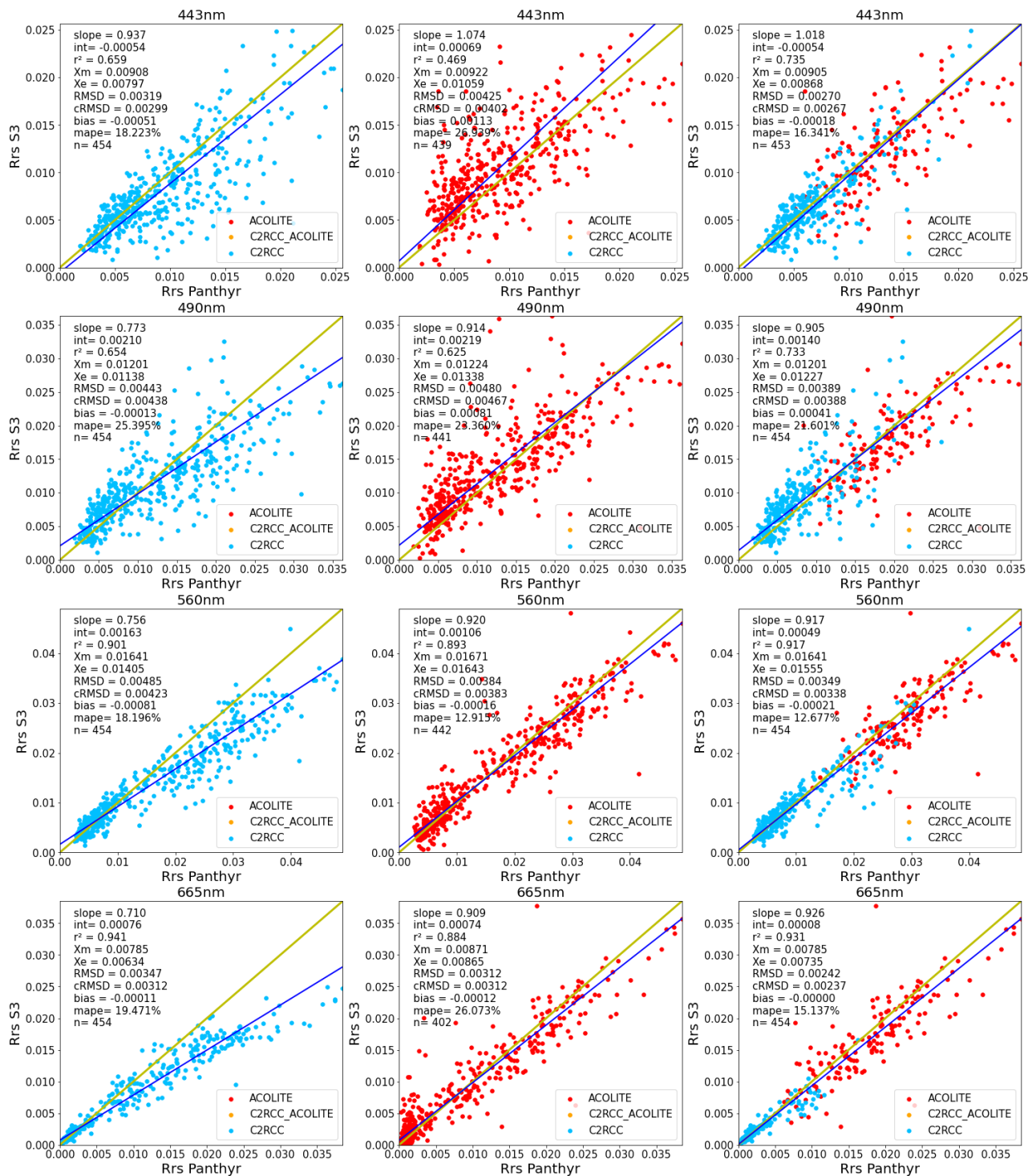
Figure 8. L3 daily MSI spectral RRS dataset in the Near-Infrared bands against in situ observations obtained from the PANTHYR network for 2 stations: RT1 and AAOT as processed with C2RCC (left column), ACOLITE-DSF (middle column) and the merged approach (right column) with a color code showing which AC was used per matchup.
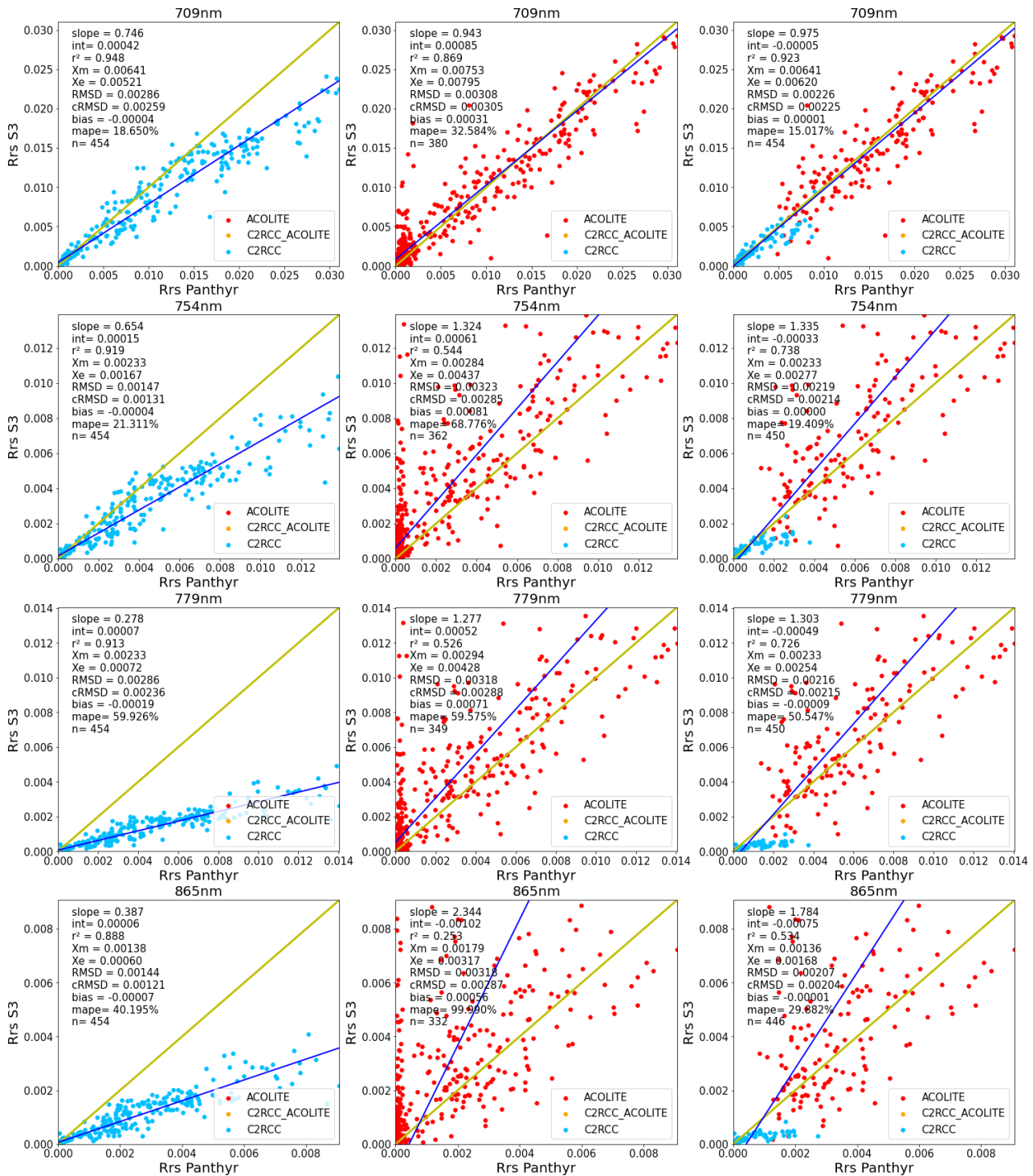
Figure 9. L3 daily OLCI spectral RRS dataset in the visual bands against in situ observations obtained from the PANTHYR network for 2 stations: RT1 and AAOT as processed with C2RCC (left column), ACOLITE-DSF (middle column) and the merged approach (right column) with a color code showing which AC was used per matchup.

Figure 10. L3 daily OLCI spectral RRS dataset in the Near-Infrared bands against in situ observations obtained from the PANTHYR network for 2 stations: RT1 and AAOT as processed with C2RCC (left column), ACOLITE-DSF (middle column) and the merged approach (right column) with a color code showing which AC was used per matchup.

Sentinel-2/MSI

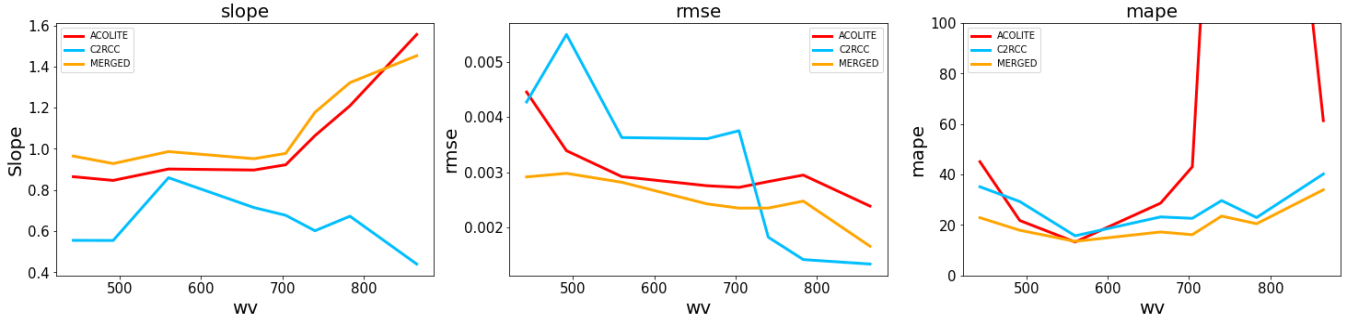Figure 11. Overview of band-specific statistical metrics as defined in table 1 for the RRS matchups between MSI products and PANTHYR observations.
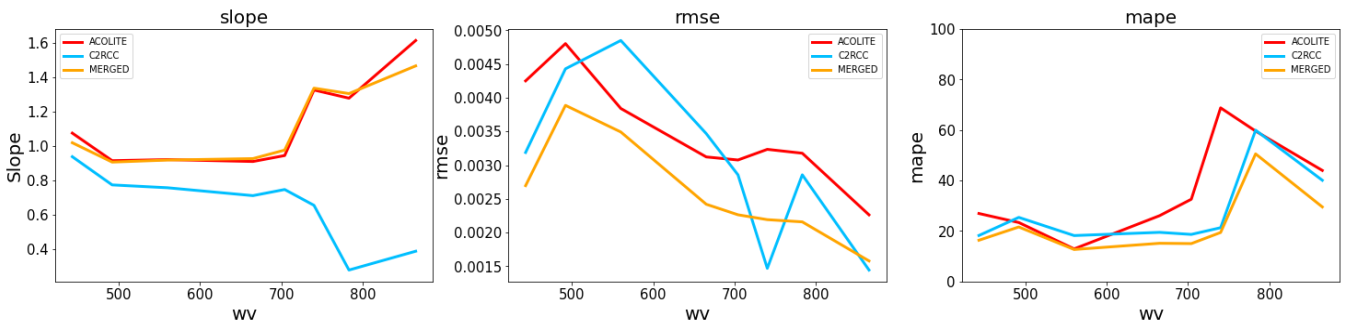
Sentinel-3/OLCI

Figure 12. Overview of band-specific statistical metrics as defined in table 1 for the RRS matchups between OLCI products and PANTHYR observations.

4. CONCLUSIONS

Both C2RCC and ACOLITE-DSF atmospheric correction algorithms are able to produce accurate RRS products for coastal applications from both Sentinel-2/MSI and Sentinel-3/OLCI sensors, each with their respective advantages and disadvantages. By using an underlying water reflectance model, C2RCC will fit the estimated RRS spectrum to a known form within the boundaries of the used training dataset [6]. This approach reduces noise in low RRS situations and generates RRS spectra that resemble water even in very challenging situations; however, it often underestimates the RRS in highly reflective scenarios. By making no assumption about the water reflectance, ACOLITE-DSF on the other hand, is able to return unusual RRS spectra corresponding to optical properties not found in a typical water reflectance model (i.e., a training dataset), complementing C2RCC where it is the less performant. Combining the two approaches yet required a comprehensive, region independent and pixel-based automatic switching scheme, along with a technique for achieving a seamless transition between the two algorithms. We here used the green-NIR ratio, which offers a clear indication of the saturation of the C2RCC outputs for the most reflective band (i.e., the RRS560), at a level where ACOLITE/DSF typically performs accurately, combined with a weighted transition between the two methods.

We exploit the unparalleled density of hyperspectral measurements provided by autonomous hyperspectral PANTHYR systems deployed in the turbid Belgian coastal waters (RT1) and complex Adriatic waters of the Gulf of Venice (AAOT) to validate the approach. Providing hyperspectral data for bands ranging from 400 to 900 nm and operational for 21 (RT1) and 32 months (AAOT), we could obtain 169 Sentinel-2/MSI matchups and 454 Sentinel-3/OLCI matchups (for the period 2019-12-11 to 2023-08-01). This represents an unprecedented dataset for evaluating ocean color satellite performance in clear and turbid coastal waters.

The C2RCC processor showed a significant underestimation of the red to NIR reflectance for highly reflective waters which means that this processor cannot be recommended for turbid water monitoring and will likely show better performance with better adapted specific water models and training data. The ACOLITE-DSF processor performed better in turbid waters but still overestimates RRS in clear waters where ACOLITE-DSF tends to underestimate the atmospheric path reflectance. This is especially noticeable where data ranges are very small (e.g. the blue 443nm band and NIR bands beyond 704nm). Matchup performance is best for the green and red channels. These findings for Sentinel-2/MSI are in line with what was presented by [2].

The best accuracies were obtained by combining the two AC procedures for bands 443nm to 709nm and this for both Sentinel-2/MSI (<21% MAPE with a 0.004 RMSD and slopes between 0.93 and 0.98) and Sentinel-3/OLCI (<23% MAPE with a 0.003 RMSD and slopes between 0.91 and 0.98). These bands generally have the highest reflectance range and are of interest for retrieving turbidity at low to moderate levels [30]. These results were obtained by applying an automatic pixel-based switching/merging approach enabling the use of the most suitable algorithm (or a combined output) based on the optical characteristics of the water at the pixel level. This merging approach maximize the ability to achieve high quality RRS spectra for a maximum number of pixels and yet retain the ability to deal with both unusual water conditions and very challenging atmospheric conditions.

The presented parametrization of the merging approach is based on currently available data from two PANTHYR stations, part of the WATERHYPERNET network (https://waterhypernet.org/) [32]. New coastal stations are in development and additional data become available in the near future which will allow us to expand this validation study to include more coastal conditions and make the parametrization more robust.

DATA AVAILABILITY

In situ data underlying the results presented in this paper are currently not publicly available but will be released in a public version later in 2023. The satellite data presented in this paper are all open access data accessible in different processing levels distributed by several data portals like the Copernicus Data Space Ecosystem (https://dataspace.copernicus.eu/), CREODIAS (https://creodias.eu/) and the Copernicus Marine service (https://marine.copernicus.eu/).

REFERENCES

[1] Novoa, S., Chust, G., Sagarminaga, Y., Revilla, M., Borja, A. and Franco, J., "Water quality assessment using satellite-derived chlorophyll-a within the European directives, in the southeastern Bay of Biscay." Marine pollution bulletin, 64(4), 739-750 (2012).

[2] Vanhellemont, Q., "Adaptation of the dark spectrum fitting atmospheric correction for aquatic applications of the Landsat and Sentinel-2 archives." Remote Sensing of Environment, 225, 175-192 (2019).

[3] Lavigne, H., Van der Zande, D., Ruddick, K., Dos Santos, J.C., Gohin, F., Brotas, V. and Kratzer, S., "Quality-control tests for OC4, OC5 and NIR-red satellite chlorophyll-a algorithms applied to coastal waters." Remote Sensing of Environment, 255, 112237 (2021).

[4] Nechad, B., Ruddick, K.G. and Neukermans, G., September. "Calibration and validation of a generic multisensor algorithm for mapping of turbidity in coastal waters." Proc. SPIE 7473, 161-171 (2009).

[5] Nechad, B., Ruddick, K.G. and Park, Y., "Calibration and validation of a generic multisensor algorithm for mapping of total suspended matter in turbid waters." Remote Sensing of Environment, 114(4), 854-866 (2010).

[6] Brockmann, C., Doerffer, R., Peters, M., Kerstin, S., Embacher, S. and Ruescas, A., "Evolution of the C2RCC neural network for Sentinel 2 and 3 for the retrieval of ocean colour products in normal and extreme optically complex waters." In Living Planet Symposium, 740, 54(2016).

[7] Doerffer, R. and Schiller, H., "The MERIS Case 2 water algorithm." International Journal of Remote Sensing, 28(3-4), 517-535 (2007).

[8] De Keukelaere, L., Sterckx, S., Adriaensen, S., Knaeps, E., Reusen, I., Giardino, C., Bresciani, M., Hunter, P., Neil, C., Van der Zande, D. and Vaiciute, D., "Atmospheric correction of Landsat-8/OLI and Sentinel-2/MSI data using iCOR algorithm: validation for coastal and inland waters." European Journal of Remote Sensing, 51(1), 525-542 (2018).

[9] Steinmetz, F., Deschamps, P.Y. and Ramon, D., "Atmospheric correction in presence of sun glint: application to MERIS." Optics express, 19(10), pp.9783-9800 (2011).

[10] Steinmetz, F. and Ramon, D., "Sentinel-2 MSI and Sentinel-3 OLCI consistent ocean colour products using POLYMER." Proc. SPIE 10778, 46-55 (2018).

[11] Pahlevan, N., Mangin, A., Balasubramanian, S.V., Smith, B., Alikas, K., Arai, K., Barbosa, C., Bélanger, S., Binding, C., Bresciani, M. and Giardino, C., "ACIX-Aqua: A global assessment of atmospheric correction methods for Landsat-8 and Sentinel-2 over lakes, rivers, and coastal waters." Remote Sensing of Environment, 258, 112366 (2021).

[12] Ruddick, K. and Lacroix, G., "Hydrodynamics and meteorology of the Belgian Coastal Zone. Current status of eutrophication in the Belgian Coastal Zone", 1-15 (2006).

[13] Neukermans, G., Ruddick, K.G. and Greenwood, N., "Diurnal variability of turbidity and light attenuation in the southern North Sea from the SEVIRI geostationary sensor." Remote Sensing of Environment, 124, 564-580 (2012).

[14] Fettweis, M. and Van den Eynde, D., "The mud deposits and the high turbidity in the Belgian–Dutch coastal zone, southern bight of the North Sea." Continental Shelf Research, 23(7), 669-691 (2003).

[15] Fettweis, M., Nechad, B. and Van den Eynde, D., "An estimate of the suspended particulate matter (SPM) transport in the southern North Sea using SeaWiFS images, in situ measurements and numerical model results." Continental Shelf Research, 27(10-11), 1568-1583 (2007).

[16] Lacroix, G., Ruddick, K., Park, Y., Gypens, N. and Lancelot, C., "Validation of the 3D biogeochemical model MIRO&CO with field nutrient and phytoplankton data and MERIS-derived surface chlorophyll a images." Journal of Marine Systems, 64(1-4), 66-88 (2007).

[17] Desmit, X., Nohe, A., Borges, A.V., Prins, T., De Cauwer, K., Lagring, R., Van der Zande, D. and Sabbe, K., "Changes in chlorophyll concentration and phenology in the North Sea in relation to de-eutrophication and sea surface warming." Limnology and Oceanography, 65(4), 828-847 (2020).

[18] Alvera-Azcárate, A., Van der Zande, D., Barth, A., Troupin, C., Martin, S. and Beckers, J.M., "Analysis of 23 years of daily cloud-free chlorophyll and suspended particulate matter in the Greater North Sea." Frontiers in Marine Science, 8, 707632 (2021).

[19] Artegiani, A., Paschini, E., Russo, A., Bregant, D., Raicich, F. and Pinardi, N., "The Adriatic Sea general circulation. Part I: Air–sea interactions and water mass structure." Journal of physical oceanography, 27(8), 1492-1514 (1997).

[20] Zavatarelli, M., Pinardi, N., Kourafalou, V.H. and Maggiore, A., "Diagnostic and prognostic model studies of the Adriatic Sea general circulation: Seasonal variability." Journal of Geophysical Research: Oceans, 107(C1), 2-1 (2002).

[21] Zibordi, G., Hooker, S.B., Berthon, J.F. and D'Alimonte, D., "Autonomous above-water radiance measurements from an offshore platform: a field assessment experiment." Journal of Atmospheric and Oceanic Technology, 19(5), 808-819 (2002).

[22] Zibordi, G., Berthon, J.F., Mélin, F., D'Alimonte, D. and Kaitala, S., "Validation of satellite ocean color primary products at optically complex coastal sites: Northern Adriatic Sea, Northern Baltic Proper and Gulf of Finland." Remote Sensing of Environment, 113(12), 2574-2591 (2009).

[23] Brando, V.E., Braga, F., Zaggia, L., Giardino, C., Bresciani, M., Matta, E., Bellafiore, D., Ferrarin, C., Maicu, F., Benetazzo, A. and Bonaldo, D., "High-resolution satellite turbidity and sea surface temperature observations of river plume interactions during a significant flood event." Ocean Science, 11(6), 909-920 (2015).

[24] Tilstone, G., Dall'Olmo, G., Hieronymi, M., Ruddick, K., Beck, M., Ligi, M., Costa, M., D'alimonte, D., Vellucci, V., Vansteenwegen, D. and Bracher, A., "Field intercomparison of radiometer measurements for ocean colour validation." Remote Sensing, 12(10), 1587 (2020).

[25] Vansteenwegen, D., Ruddick, K., Cattrijsse, A., Vanhellemont, Q. and Beck, M., "The pan-and-tilt hyperspectral radiometer system (PANTHYR) for autonomous satellite validation measurements—Prototype design and testing." Remote Sensing, 11(11), 1360 (2019).

[26] Ruddick, K.G., De Cauwer, V., Park, Y.J. and Moore, G., "Seaborne measurements of near infrared water-leaving reflectance: The similarity spectrum for turbid waters." Limnology and Oceanography, 51(2), 1167-1179 (2006).

[27] Mobley, C.D., "Estimation of the remote-sensing reflectance from above-surface measurements." Applied optics, 38(36), 7442-7455 (1999).

[28] Vanhellemont, Q. and Ruddick, K., "Atmospheric correction of Sentinel-3/OLCI data for mapping of suspended particulate matter and chlorophyll-a concentration in Belgian turbid coastal waters." Remote Sensing of Environment, 256, 112284 (2021).

[29] Vanhellemont, Q., "Sensitivity analysis of the dark spectrum fitting atmospheric correction for metre-and decametre-scale satellite imagery using autonomous hyperspectral radiometry." Optics Express, 28(20), 29948-29965 (2020).

[30] Novoa, S., Doxaran, D., Ody, A., Vanhellemont, Q., Lafon, V., Lubac, B. and Gernez, P., "Atmospheric corrections and multi-conditional algorithm for multi-sensor remote sensing of suspended particulate matter in low-to-high turbidity levels coastal waters." Remote Sensing, 9(1), 61 (2017).

[31] Bailey, S.W. and Werdell, P.J., "A multi-sensor approach for the on-orbit validation of ocean color satellite data products. Remote sensing of environment", 102(1-2), 12-23 (2006).

[32] Ruddick, K. Beck, M., Bialek, A., Brando, V. Cattrijsse, A., Concha, J., Corizzi, A., de Vis, P., Dogliotti, A., Doxaran, D., Gammaru, A., Giardino, C., Gonzales Vilas, L., Goyens, C., Hunt, S., Kuusk, J., Laizans, K., Leymarie, E., Ortenzio, F., Piegari, E., Perna, P., Rubinstein, L., Vanhellemont, Q. and Vansteenwegen, D. "WATERHYPERNET: Automated in situ measurements of hyperspectral water reflectance for satellite validation ... and more.", Proc. Oceans from Space V, 68-69 (2022).